5

NUMERICAL STUDY ON TRANSITION PREDICTION METHOD AND EXPERIMENTAL STUDY ON EFFECT OF SUPERSONIC LAMINAR FLOW CONTROL

Kenji YOSHIDA and Hirokage OGOSHI
Gifu Technical Institute
Kawasaki heavy Industries , Ltd.
Kakamigahara , Gifu , Japan
Youji ISHIDA and Masayosi NOGUCHI
Aircraft Aerodynamics Division
National Aerospace Laboratory
Tokyo , Japan

ABSTRACT

To develop an aerodynamic design system applying supersonic laminar flow control (SLFC) , numerical study on a transition prediction method and experimental study on the effect of SLFC were performed . In the first phase of our study , we developed an analysis system of linear stability and then obtained good validation for the estimated amplification rate in several typical cases . In the second phase , we developed a transition prediction system by applying an empirical e^N method and then obtained good validation for the estimated N-factor in two typical cases . In the third phase , we carried out wind tunnel tests using an originally designed warped delta wing model , to obtain some data of transition and the effect of SLFC under supersonic flow condition . And finally we tried to analyze the transition characteristics of our model and obtained the useful result of $N \fallingdotseq 7$ at transition at Mach 1.4 .

1. INTRODUCTION

It is well known that laminar flow control (LFC) is one of the most effective technologies for improving aerodynamic characteristics of a transport aircraft , for example , a next generation SST . To develop the aerodynamic design system with supersonic laminar flow control (SLFC) , it is , first of all , necessary to understand transition phenomenon in a 3-dimensional compressible boundary layer . But such phenomenon is more difficult than that in a low speed boundary layer . The reason is based on the complexity due to the compressibility , 3-dimensionality , and nonlinearity . Even now there is little useful experimental data and information on SLFC , because of such difficulties .

As a first step , therefore , we started to investigate such transition phenomenon of a 3-dimensional compressible boundary layer numerically and experimentally . In the numerical approach , to understand the physical mechanism of the transition phenomenon , we analyzed linear stability characteristics and estimated transition position by using the empirical e^N method . On the other hand , in the experimental approach , to obtain some c data in developing the design

system with SLFC , we carried out wind tunnel tests on SLFC in cooperation with NAL , using a model with a suction system .

Our study consists of 3 phases . In the first phase , we derived the formulation on linear stability of a 3-dimensional compressible boundary layer c to the spatial theory[1,2] , and developed a system for calculating the eigenvalue and amplification rate of small disturbances . Then we validated it in several typical cases by comparing our estimated amplification rates with those by other workers . In the second phase , we investigated the spatial growth of amplification rate and developed a transition prediction method based on the empirical e^N method . This method consists of calculating the "N-factor" through the integration of several amplification rates and comparing it with the empirically obtained N-value which corresponds to the transition of the boundary layer . In the third phase , we carried out wind tunnel tests using an originally designed warped delta wing model and obtained some useful data for the transition and the effect of SLFC . Then we tried to analyze the transition characteristics of our test model using the present prediction method .

The purpose of this paper is to summarize the principal results of our study . The results of the first , second and third phase are described in section 2 , 3 and 4 respectively .

2. STUDY ON LINEAR STABILITY OF 3-DIMENSIONAL COMPRESSIBLE BOUNDARY LAYER

2.1 Formulation

1) Basic equation

Present formulation is based on the following assumptions .

① simple plane wave disturbances

$$\{u',v',w',p',T',\rho',\mu'\} \equiv q'(x,y,z,t) = \tilde{q}(y)\, e^{i(\alpha x+\beta z-\omega t)}$$

Here (x,y,z) are the coordinates of streamwise direction , thickness direction of boundary layer and spanwise direction , (u,v,w) the (x,y,z) components of velocity , (p,T,ρ,μ) a pressure , temperature , density and viscosity respectively . And ω is a circular frequency (real) and α,β the components of wave number vector (complex) .

② parallel mean flow

$$\{U,V,W,P,T,\rho,\mu\} = \{U(y),0,W(y),1,T(y),\rho(y),\mu(y)\}$$

Then the basic equation generally can be summarized in the following form [1,2] .

$$\frac{d\varphi_i}{dy} = \sum_{j=1}^{8} a_{ij}\,\varphi_j \quad , \quad i = 1,8 \qquad (1)$$

where $\varphi_1 = \alpha\tilde{u} + \beta\tilde{w}$, $\varphi_2 = \dfrac{d\varphi_1}{dy}$, $\varphi_3 = \tilde{v}$, $\varphi_4 = \tilde{p}$,

$\varphi_5 = \tilde{T}$, $\varphi_6 = \dfrac{d\varphi_5}{dy}$, $\varphi_7 = \alpha\tilde{w} - \beta\tilde{u}$, $\varphi_8 = \dfrac{d\varphi_7}{dy}$

Here these quantities are non-dimensionalized with boundary layer thickness and reference quantities at the edge of boundary layer . And the matrix a_{ij} is related to the boundary layer

profiles of velocity , temperature , etc. . Those details are described in Appendix I .

2) Boundary condition

Generally the boundary condition in linear stability analysis is that all disturbances vanish at the wall and the edge of the boundary layer as follows :

$$\varphi_1 = \varphi_3 = \varphi_5 = \varphi_7 = 0 \quad , \quad at\ y = 0$$
$$\varphi_1 \, , \, \varphi_3 \, , \, \varphi_5 \, , \, \varphi_7 \to 0 \quad , \quad as\ y \to \infty \qquad (2)$$

Here the combination of the above homogeneous basic equation and such boundary condition leads to trivial solutions , except for only one case where each parameter of the matrix is equal to the eigenvalue respectively . Therefore we must solve the so-called eigenvalue problem .

2.2 Method of Solution

To solve this eigenvalue problem , we adapted the method described in ref.2 . The details are summarized in Appendix III and the main features are as follows :

① Integration from edge to wall by the 4th order Runge-Kutta-Gill method

② Application of analytical solution on the initial values at the edge (see Appendix II)

③ Use of the orthonormalization technique by Gram-Schmidt[3] to remove the errors due to numerical integration (see Appendix IV)

④ Iteration by the Newton method with a "pseudo" boundary condition

2.3 Validation of Present Formulation

As a first step , we tried to validate present formulation in two typical cases .

1) 2-dimensional incompressible viscous flow

First of all , under the assumptions of 2-dimensionality and incompressibility , the following relations are obtained :

$$W = \frac{dW}{dy} = 0 \quad , \quad \tilde{w} = 0 \quad \Rightarrow \quad \varphi_1 = \alpha \tilde{u} \quad , \quad \varphi_7 = -\beta \tilde{u} \qquad (3)$$

$$\beta = 0 \quad \Rightarrow \quad \varphi_7 = \varphi_8 = 0 \qquad (4)$$

$$T \, , \, \frac{dT}{dy} \quad : \text{unnecessary} \quad \Rightarrow \quad \varphi_5 = \varphi_6 \quad : \text{unnecessary} \qquad (5)$$

Then we can derive the governing equation for $\varphi_3 = \tilde{v}$ from eq. (1) as follows :

$$\left\{ \frac{1}{R}\left(\frac{d^2}{dy^2} - \alpha^2 \right)^2 - i(\alpha U - \omega)\left(\frac{d^2}{dy^2} - \alpha^2 \right) + i\alpha \frac{d^2 U}{dy^2} \right\} \varphi_3 = 0 \qquad (6)$$

This is completely equal to the well-known Orr-Sommerfeld equation

2) 2-dimensional compressible inviscid flow

Next , under the assumptions of 2-dimensionality (3) and 3-dimensional disturbance ($\beta \neq 0$) , the following inviscid condition is added :

$$\mu = \frac{d\mu}{dy} = \frac{d\mu}{dT} = 0 \quad , \quad R \to \infty \tag{7}$$

Then we can derive the governing equation for $\varphi_4 = \tilde{p}$ from eq. (1) as follows :

$$\left\{ \frac{d^2}{dy^2} - \frac{d}{dy}(\ln \tilde{M}^2) \frac{d}{dy} - (\alpha^2 + \beta^2)(1 - \tilde{M}^2) \right\} \varphi_4 = 0 \quad , \quad \tilde{M} \equiv \frac{(\alpha U - \omega) M_e}{\sqrt{(\alpha^2 + \beta^2) T}} \tag{8}$$

This is completely equal to the equation derived by Lees & Lin [4] and Mack [5] .

2.4 Numerical Validation

As the next step , we numerically investigated eigenvalue characteristics in some typical cases .

1) 2-dimensional disturbance on flat plate boundary layer

First of all , we analyzed a case of incompressible flat plate , namely Blasius boundary layer , and obtained the result summarized in Fig.1 . This figure shows the comparison of a neutral curve between the present estimation and the famous solution by Tollmien-Schlichting . Here the abscissa indicates Reynolds number based on displacement thickness δ^* and the ordinate denotes the wave number of disturbance which is non-dimensionalized with δ^* As seen in this figure , we obtained good agreement .

Next we analyzed some compressible cases and summarized the results in Fig.2 and 3 , comparing with the results by Arnal[6] . Fig.2 shows several eigenvalues corresponding to stable or unstable states of the boundary layer at Mach 2.2 in the plane of Reynolds number and wave number . And Fig.3 shows the neutral curve on the boundary layer at Mach 3.0 . As seen in these figures , we could mostly obtain good agreement .

2) 3-dimensional disturbance on flat plate boundary layer

As a typical case including 3-dimensionality , first of all , we investigated the maximum amplification rate of 3-dimensional disturbance on the 2-dimensional compressible flat plate boundary layer , and obtained the result shown in Fig.4 . Here the abscissa indicates the Mach number of the mean flow , and the ordinate denotes maximum amplification rate . And ψ is the angle between the directions of mean flow and propagation of disturbance . As seen in this figure , we obtained good agreement with the result by Mack[5] .

3) 2-dimensional disturbance on Falkner-Skan-Cooke boundary layer

As the next case on 3-dimensionality , we investigated 2-dimensional disturbance on the boundary layer of simple 3-dimensional flow over an infinite swept wing with a wedge-shaped cross-section . Usually the characteristics of the boundary layer on this wing are predicted by the solution of the well-known Falkner-Skan-Cooke boundary layer equation[7] .

Fig.5 shows the relation between maximum amplification rate and sweep angle , compared with the result by Mack[1] . Here the abscissa indicates sweep angle and the ordinate denotes the maximum

amplification rate divided by the value for the Blasius boundary layer. As seen in this figure, we could not obtain good agreement quantitatively but found it qualitatively. Presently we are considering that the quantitative difference originated in a numerical error in the calculation of boundary layer profiles.

3. STUDY ON TRANSITION PREDICTION METHOD

Recently it is well known that the current e^N method is widely used to predict the transition position. This method consists of the following two parts. The first part consists of estimating the amplification rates of several disturbances, and the other consists of comparing the integrated amplification rates called "N-factor", with a specified value derived empirically according to a lot of experimental data on transition. In this study, we first investigated the formulation of the e^N method and then validated it through typical numerical analysis.

3.1 Formulation of the e^N Method

1) Definition of amplitude of disturbance

According to the assumption of small plane wave disturbance, the amplitude A on 3-dimensional disturbance is defined as follows :

$$\ln\left(\frac{A}{A_0}\right) = \int_C \left(-\alpha_i dx_s - \beta_i dy_s\right) = \int_C d\sigma \tag{9}$$

where A_0 is the amplitude at the neutral point. Here in this formulation, for convenience we adapted the so-called streamline coordinate, which is different from that in previous stability formulations. That is, the direction of the streamline at the edge of the boundary layer is indicated by x_s, the direction of cross-flow y_s.

2) Assumption for the amplification of disturbance

Unless the path for integration is specified, we can not calculate the above integration. Moreover some supplementary relations between wave number (α_r, β_r) and amplification rate (α_i, β_i) are necessary. Presently some models are suggested to solve this problem. Through detailed investigation of these models, we decided to adapt the following approach :

According to the assumption of specifying the amplification direction (θ) suggested by Mack, first of all, we can simplify the formulation as follows :

$$\frac{dy_s}{dx_s} = \tan\theta \quad , \quad \beta_i = \alpha_i \tan\bar{\psi} \quad \Rightarrow \quad d\sigma = -\alpha_i(1 + \tan\bar{\psi}\tan\theta)dx_s \tag{10}$$

Here $\bar{\psi}$ is treated as a parameter.

Then we assume $\theta = 0$, because this assumption simplifies the present method and it is physically reasonable to consider that the most dominate direction is the streamline direction. And finally we obtain the following relation.

$$d\sigma = -\alpha_i dx_s = -\frac{\alpha_i}{\cos\phi_e} dx_c \tag{11}$$

where x_c stands for the coordinate in the chordwise direction normal to the leading edge and ϕ_e the local sweep angle at the edge. On the other hand, $\bar{\psi}$ is not explicitly included in this expression, but the influence of $\bar{\psi}$, namely β_i is implicitly reflected by $\alpha_i(\psi, \bar{\psi}, f, R(x_c))$. Here $\psi \equiv \tan^{-1}\left(\frac{\beta_r}{\alpha_r}\right)$, $f = \frac{\omega}{2\pi}$

3) Method to estimate N-factor

Presently it is known that there are several methods to estimate the N-factor based on the above definition of the amplitude of disturbance. Among them, we adapted the following Envelop Method[8].

$$N = \underset{\psi}{Max}\ \underset{\bar{\psi}}{Max}\ \underset{f}{Max}\left[\ln\left(\frac{A}{A_0}\right)_{\psi,\bar{\psi},f}\right] \tag{12}$$

$$\ln\left(\frac{A}{A_0}\right)_{\psi,\bar{\psi},f} = \int_C d\sigma = \int_{x_{c0}}^{x_c} \frac{-\alpha_i(x_c;\psi,\bar{\psi},f)}{\cos\phi_e(x_c)} dx_c = \int_{\xi_{c0}}^{\xi_c} \frac{f(x_c;\psi,\bar{\psi},f)}{\cos\phi_e} d\xi \tag{13}$$

$$f(x_c;\psi,\bar{\psi},f) \equiv -\alpha_i(x_c;\psi,\bar{\psi},f)\cdot\delta(x_c) \quad , \quad \xi_c \equiv \frac{x_c}{\delta}$$

Here $\underset{\psi}{Max}, \underset{\bar{\psi}}{Max}, \underset{f}{Max}$ stand for choosing local maximum values for $\psi, \bar{\psi}, f$ at each x_c respectively. Therefore N corresponds to the envelop for every curve.

3.2 Validation of Present e^N Method

To validate our e^N method, we investigated transition characteristics in the following two cases.

1) 2-dimensional incompressible flat plate flow (Blasius flow)

First of all, we analyzed the relation between amplification rate $(-\alpha_i\delta)$ and frequency (f) in the range of various Reynolds number based on boundary layer thickness (Rd), using our linear stability formulation. One of those results is shown in Fig. 6. Then using these relations, we summarized the estimated N-factor as shown in the lower part of Fig. 7. Here the upper part of this figure shows the result by Arnal[8]. In a comparing them, we obtained good agreement. And since it is experimentally observed that the natural transition exists in the range indicated by the black arrow in Fig. 7, we can estimate that the N-factor corresponding to the transition is about 8 to 10.

2) 3-dimensional incompressible infinite swept flat plate flow

For another validation, we investigated the wind tunnel test on a swept flat plate carried out at DFVLR[9]. In the analysis of such a flow field, the so-called Falkner-Skan-Cooke boundary

layer approach is approximately effective. Therefore, using this approach, we estimated the N-factor and summarized the result in the lower part of Fig. 8. Here the upper part shows the result estimated by DFVLR using temporal theory. As seen in this figure, we obtained good agreement except for lower frequencies.

Since in ref. 9 it is stated that transition was not observed in the test because of a weak adverse pressure gradient, we can estimate that the transition N-factor is more than 12.

4. STUDY ON WIND TUNNEL TESTS FOR SUPERSONIC LAMINAR FLOW CONTROL

The main objective of our wind tunnel tests is to obtain some useful data for understanding transition phenomenon at supersonic speed and developing a transition prediction system including the effect of SLFC. Therefore we originally designed a wing model with the suction system for SLFC and carried out the tests at the 2m×2m transonic wind tunnel of the National Aerospace Laboratory (NAL). Then we analyzed the transition characteristics using our prediction system and compared the estimated result with the test result.

4.1 Wind Tunnel Test

1) Outline of present wind tunnel tests

Our tunnel model is a half-mounted wing model, as shown in Fig. 9, and it has a special upper surface with about 60,000 tiny holes (0.1 mm diameter) for suction of air. Its planform is a simple one, namely delta shaped, but its surface is a little complicated, because the "warped surface", which was designed originally for minimizing lift-dependent drag, is applied to this model.

We carried out wind tunnel test twice. As our attention is directed to supersonic speed, the test case at M=1.4 was emphasized. In those tests, we measured force and pressure on the surface and in the wake. Also we tried to obtain the transition characteristics by using two visualization techniques, that is, monitoring by an infrared camera and a liquid crystal.

Our wind tunnel tests consist of the following three parts. The first part is a "fundamental test" to obtain the fundamental characteristics of our model. The second part is a "suction test" to investigate the effect on the suction of the boundary layer. And the third part is a "visualization test" to understand the transition characteristics.

2) Summary of test results

In the fundamental test, since we obtained good agreement between the estimated and measured pressure distributions under design conditions, we validated our warped surface design method. However, the influence of the tunnel wall was made clear by the reduction of lift slope.

In the suction test, we couldn't find any significant effect in either the characteristics of total drag or the distribution of total pressure loss in the wake. And presently we are considering that the reason is based on (1) a stronger cross flow instability than we had

predicted and (2) the small suction surface . Therefore we need to improve our model to obtain useful data on SLFC .

In the visualization test , using the liquid crystal technique , we observed the natural transition in the condition of the existing accelerated region on the forward part of the lower surface . This condition was chosen to realize the delay of the natural transition . (Here the reason why we didn't give the upper surface a coat of liquid crystal is based on the existence of the suction surface .) The natural transition characteristics obtained through the other pattern of liquid crystal is summarized in Fig. 10 . As seen in this figure , we found that the location of transition was about 6% local chord length at the condition of M=1.4 and α=8°

On the other hand , in the test with an infrared camera , we couldn't clearly observe the natural transition . Presently we are considering that the reason is based on the influence of other sources , for example , lighting , porous wall , beams , etc.. Therefore at the next step , such surrounding should be improved as much as possible .

4.2 Study of Transition Characteristics Based on Test Results

As one validation of our transition prediction method , we investigated the transition characteristics of the present wind tunnel model . First of all , we analyzed the 3-dimensional compressible laminar boundary layer based on the measured pressure distribution , using the method described in ref. 10 . Then we solved the eigenvalue problem and estimated the N-factor .

The results are as follows .

1) Influence of $\bar{\psi}$

As there are some parameters such as f, ψ and $\bar{\psi}$ in our method , the influence of these parameters on the amplification rate of disturbance should be investigated in detail . First of all , we investigated the influence of $\bar{\psi}$.

Generally we have supposed that the transition phenomenon of our model is mainly dominated by cross flow instability , because of its highly swept leading edge . Therefore we paid attention to the case of $\psi \fallingdotseq 70 \sim 90°$. Consequently we found that the amplification rate had the largest value at the condition of $\bar{\psi} = 0°$.

2) Influence of ψ

Next we investigated the influence of ψ in the condition of $\bar{\psi} = 0°$. And we ascertained that the amplification rate at $\psi > 0°$ was larger than that at $\psi < 0°$. This is easily understandable when considering the relation between the sweep angle and the direction of cross flow . Therefore the condition of $0° < \psi < 90°$ is enough for the present analysis .

3) Estimation of N-factor

Fig. 11 shows the estimated N-factor on the lower surface of our model at the condition of

M=1.4, α=8° and 40% semi-span position. As seen in this figure, the disturbance with f =60 kHz generates the largest N near the region of the leading edge, and the disturbance with f=40 kHz does so at the rear part.

Generally, in the e^N method, the location of transition is predicted by comparing the estimated N-factor with the empirical N value corresponding to the transition. For a 3-dimensional compressible boundary layer, however, the reasonable value of transition N-factor has not been estimated empirically yet. Therefore, in this stage, we can't completely predict the location of transition. It is very important to gather a lot of experimental data to estimate the reasonable N value. And from this standpoint, we tried to estimate the N value based on the present test result.

In our liquid crystal visualization test, it was observed that the transition was located at a position about 6% local chord rearward from the leading edge. Therefore we can estimate that the transition N value is nearly equal to 7. This value is less than the N value of 8 to 10 usually used on 2-dimensional incompressible flat plate flows, as we mentioned above. Here we consider that this value is roughly valid, because of the fact that the transition Reynolds number on a compressible boundary layer is generally less than on an incompressible one.

But present estimation is not extremely precise because of the existence of some factors influencing transition, such as turbulence of the freestream, the number in the porous wall, the boundary layer on the tunnel wall, and so on. Therefore a lot of wind tunnel tests should be carried out using several models of which the transition position is well known.

5. CONCLUDING REMARKS

As a first step in developing a design system for supersonic laminar flow control (SLFC), we first investigated the linear stability of the 3-dimensional compressible boundary layer and then developed a transition prediction system according to the current e^N method. Next we carried out wind tunnel tests using the model designed originally for SLFC, to understand the effect of SLFC and to obtain useful data for it. Unfortunately, though the effect of SLFC wasn't made clear because of the large swept angle and small suction surface of our model, we could obtain information on the natural transition through the visualization test using a liquid crystal. Then comparing this test result with the analysis for the transition of our model by the present method, we ascertained that the transition N value was about 7. To improve the precision of present estimation, however, it is necessary to continue further study in wind tunnel tests.

REFERENCES

1) L.M. Mack : " Boundary-Layer Linear Stability Theory ", Special Course on Stability and Transition of Laminar Flow, AGARD Rep. No.709, 3-1~81, 1984

2) N.M. El-Hady : " Nonparallel Stability of Three-Dimensional Compressible Boundary Layers , Part I - Stability Analysis " , NASA CR-3245 , 1980
3) Tatsumi , Gotoh : "Stability Theory of Flow " , Sangyou Tosyo, 1976
4) L. Lees and C.C. Lin : " Investigation of The Stability of The Laminar Boundary Layer in A Compressible Fluid " , NACA TN-1115 , 1946
5) L.M. Mack : "Linear Stablilty Theory and the Problem of Supersonic Boundary-Layer Transition " , AIAA J. Vol.13 , No.3 , pp.278-289 , 1975
6) D. Arnal : " Stability and Transition of Two-Dimensional Laminar Boundary Layers in Compressible Flow over An Adiabatic Wall " , La Recherche Aerospatiale No.1988-4
7) L. Rosenhead (Ed.) : " Laminar Boundary Layer " , Dover Publications Inc., 1961
8) D. ARNAL : " Boundary layer transition : prediction based on linear theory " , AGARD FDP/VKI Special Course on Progress in Transition Modelling , AGARD Report 793 , 1993
9) F. Meyer and L. Kleiser : "Numerical Investigation of Transition in 3D Boundary Layers , AGARD-CP-438 , 16-1 , 1989
10) T. Cebeci , K. Kaups and J.A. Ramsey : NASA CR-2777

APPENDIX I . DETAIL EXPRESSION FOR THE MATRIX $\{a_{ij}\}$

In the following expression , R denotes the Reynolds number based on velocity , density , viscosity at the edge of boundary layer respectively and boundary layer thickness , and γ , σ and M_e indicate the ratio of specific heat (=1.4) , Prandtl number and Mach number at the edge of boundary layer , respectively .

$$\{a_{ij}\} = \begin{pmatrix} 0 & 1 & 0 & 0 & 0 & 0 & 0 & 0 \\ a_{21} & a_{22} & a_{23} & a_{24} & a_{25} & a_{26} & 0 & 0 \\ -i & 0 & a_{33} & a_{34} & a_{35} & 0 & 0 & 0 \\ a_{41} & a_{42} & a_{43} & a_{44} & a_{45} & a_{46} & 0 & 0 \\ 0 & 0 & 0 & 0 & 0 & 1 & 0 & 0 \\ 0 & a_{62} & a_{63} & a_{64} & a_{65} & a_{66} & 0 & a_{68} \\ 0 & 0 & 0 & 0 & 0 & 0 & 0 & 1 \\ 0 & 0 & a_{83} & 0 & a_{85} & a_{86} & a_{87} & a_{88} \end{pmatrix} \tag{A1}$$

$$a_{21} = i\rho\frac{R}{\mu}(\alpha U + \beta W - \omega) + \alpha^2 + \beta^2$$

$$a_{22} = -\frac{1}{\mu}\frac{d\mu}{dy}$$

$$a_{23} = \frac{\rho R}{\mu}\left(\alpha\frac{dU}{dy} + \beta\frac{dW}{dy}\right) + (\alpha^2 + \beta^2)\left(-\frac{i}{3T}\frac{dT}{dy} - \frac{i}{\mu}\frac{d\mu}{dy}\right)$$

$$a_{24} = (\alpha^2 + \beta^2)\left\{\frac{iR}{\mu} - \frac{(\alpha U + \beta W - \omega)\gamma M_e^2}{3\rho T}\right\}$$

$$a_{25} = \frac{(\alpha U + \beta W - \omega)(\alpha^2 + \beta^2)}{3T} - \frac{1}{\mu}\frac{\partial}{\partial y}\left\{\frac{d\mu}{dT}\left(\alpha\frac{dU}{dy} + \beta\frac{dW}{dy}\right)\right\}$$

$$a_{26} = -\frac{1}{\mu}\frac{d\mu}{dT}\left(\alpha\frac{dU}{dy} + \beta\frac{dW}{dy}\right)$$

$$a_{33} = \frac{1}{T}\frac{dT}{dy}$$

$$a_{34} = -\frac{i}{\rho}(\alpha U + \beta W - \omega)\frac{\gamma M_e^2}{T}$$

$$a_{35} = \frac{i}{T}(\alpha U + \beta W - \omega)$$

$$a_{41} = \frac{1}{1+c}\left\{-\frac{i}{R}\left(\frac{4\mu}{3T}+2\frac{d\mu}{dT}\right)\frac{dT}{dy}\right\} \quad , \quad c \equiv \frac{4}{3}\frac{i\gamma M_e^{\,2}\mu(aU+\beta W-\omega)}{\rho RT}$$

$$a_{42} = \frac{1}{1+c}\left(-\frac{i\mu}{R}\right)$$

$$a_{43} = \frac{1}{1+c}\left[\frac{4\mu}{3RT}\left\{\frac{d^2T}{dy^2}+\frac{1}{\mu}\frac{d\mu}{dT}\left(\frac{dT}{dy}\right)^2\right\}-i\rho(aU+\beta W-\omega)-\frac{\mu}{R}(\alpha^2+\beta^2)\right]$$

$$a_{44} = -\frac{1}{1+c}\frac{4}{3}\frac{i\gamma M_e^{\,2}\mu}{\rho RT}\left\{\left(\frac{1}{\mu}\frac{d\mu}{dT}+\frac{1}{T}\right)\frac{dT}{dy}(aU+\beta W-\omega)+\alpha\frac{dU}{dy}+\beta\frac{dW}{dy}\right\}$$

$$a_{45} = \frac{1}{1+c}\left\{\frac{4}{3}\frac{i(aU+\beta W-\omega)}{RT}\frac{d\mu}{dT}\frac{dT}{dy}+i\left(\frac{4\mu}{3RT}+\frac{1}{R}\frac{d\mu}{dT}\right)\left(\alpha\frac{dU}{dy}+\beta\frac{dW}{dy}\right)\right\}$$

$$a_{46} = \frac{1}{1+c}\frac{4}{3}\frac{i\mu(aU+\beta W-\omega)}{RT}$$

$$a_{62} = -2(\gamma-1)\sigma M_e^{\,2}\frac{1}{\alpha^2+\beta^2}\left(\alpha\frac{dU}{dy}+\beta\frac{dW}{dy}\right)$$

$$a_{63} = \frac{\sigma R\rho}{\mu}\frac{dT}{dy}-2i(\gamma-1)\sigma M_e^{\,2}\left(\alpha\frac{dU}{dy}+\beta\frac{dW}{dy}\right)$$

$$a_{64} = -i(\gamma-1)M_e^{\,2}\frac{\sigma R}{\mu}(\alpha U+\beta W-\omega)$$

$$a_{65} = i\frac{\sigma R\rho}{\mu}(\alpha U+\beta W-\omega)-\frac{(\gamma-1)\sigma M_e^{\,2}}{\mu}\frac{d\mu}{dT}\left\{\left(\frac{dU}{dy}\right)^2+\left(\frac{dW}{dy}\right)^2\right\}-(\alpha^2+\beta^2)-\frac{1}{\mu}\frac{d^2\mu}{dy^2}$$

$$a_{66} = -\frac{2}{\mu}\frac{d\mu}{dy}$$

$$a_{68} = -2(\gamma-1)\sigma M_e^{\,2}\frac{1}{\alpha^2+\beta^2}\left(\alpha\frac{dW}{dy}-\beta\frac{dU}{dy}\right)$$

$$a_{83} = \frac{\rho R}{\mu}\left(\alpha\frac{dW}{dy}-\beta\frac{dU}{dy}\right)$$

$$a_{85} = -\frac{1}{\mu}\frac{d}{dy}\left\{\frac{d\mu}{dT}\left(\alpha\frac{dW}{dy}-\beta\frac{dU}{dy}\right)\right\}$$

$$a_{86} = -\frac{1}{\mu}\frac{d\mu}{dT}\left(\alpha\frac{dW}{dy}-\beta\frac{dU}{dy}\right)$$

$$a_{87} = a_{21}$$

$$a_{88} = -\frac{1}{\mu}\frac{d\mu}{dy}$$

APPENDIX II. ANALYTICAL SOLUTION AT THE EDGE OF BOUNDARY LAYER

At the edge of boundary layer , the following relation is generally specified .

$$\{U,W,T,\rho,\mu\}=\{1,W_1,1,1,1\} \tag{A2}$$

And all derivatives on y are equal to 0 . Then all components of the matrix $\{a_{ij}\}$ are constant and simplified as follows :

$$\{a_{ij}(y \geq \delta)\} \equiv \{\bar{a}_{ij}\} = \begin{pmatrix} 0 & 1 & 0 & 0 & 0 & 0 & 0 & 0 \\ \bar{a}_{21} & 0 & 0 & \bar{a}_{24} & \bar{a}_{25} & 0 & 0 & 0 \\ -i & 0 & 0 & \bar{a}_{34} & \bar{a}_{35} & 0 & 0 & 0 \\ 0 & \bar{a}_{42} & \bar{a}_{43} & 0 & 0 & \bar{a}_{46} & 0 & 0 \\ 0 & 0 & 0 & 0 & 0 & 1 & 0 & 0 \\ 0 & 0 & 0 & \bar{a}_{64} & \bar{a}_{65} & 0 & 0 & 0 \\ 0 & 0 & 0 & 0 & 0 & 0 & 0 & 1 \\ 0 & 0 & 0 & 0 & 0 & 0 & \bar{a}_{87} & 0 \end{pmatrix} = const. \tag{A3}$$

If we consider the basic equation above the edge , we can derive the next equation .

$$\frac{d\bar{\varphi}_i}{dy} = \sum_{j=1}^{8} \bar{a}_{ij}\,\bar{\varphi}_j \quad , \quad i = 1 \sim 8 \tag{A4}$$

where $\bar{\varphi}_i \equiv \varphi_i(y \geq \delta)$.

Using the eigenvalues and eigenfunctions of the matrix $\{\bar{a}_{ij}\}$, we can obtain the solution $\bar{\varphi}_i$ of this equation analytically in accordance with the following procedure .

First of all , introducing Equation (A4) ,

$\psi_1 = \bar{\varphi}_1$, $\psi_2 = \bar{\varphi}_4$, $\psi_3 = \bar{\varphi}_5$ *and* $\psi_4 = \bar{\varphi}_7$ is rewritten as follows :

$$\frac{d^2}{dy^2}\begin{pmatrix}\psi_1\\ \psi_2\\ \psi_3\\ \psi_4\end{pmatrix} = \begin{pmatrix} A_{11} & A_{12} & A_{13} & 0 \\ 0 & A_{22} & A_{23} & 0 \\ 0 & A_{32} & A_{33} & 0 \\ 0 & 0 & 0 & A_{44} \end{pmatrix}\begin{pmatrix}\psi_1\\ \psi_2\\ \psi_3\\ \psi_4\end{pmatrix} \tag{A5}$$

where

$$A_{11} = \bar{a}_{21} \quad , \quad A_{12} = \bar{a}_{24} \quad , \quad A_{13} = \bar{a}_{25}$$

$$A_{22} = \bar{a}_{42}\bar{a}_{24} + \bar{a}_{43}\bar{a}_{34} + \bar{a}_{46}\bar{a}_{64} \quad , \quad A_{23} = \bar{a}_{42}\bar{a}_{25} + \bar{a}_{43}\bar{a}_{35} + \bar{a}_{46}\bar{a}_{65}$$

$$A_{32} = \bar{a}_{64} \quad , \quad A_{33} = \bar{a}_{65}$$

$$A_{44} = A_{11}$$

Next if we assume a typical solution such as $\psi \propto e^{\lambda y}$, we can analytically obtain the eigenvalues λ_i of the matrix $\{A_{ij}\}$ through the following eigenvalue equation .

$$\begin{vmatrix} A_{11}-\lambda^2 & A_{12} & A_{13} & 0 \\ 0 & A_{22}-\lambda^2 & A_{23} & 0 \\ 0 & A_{32} & A_{33}-\lambda^2 & 0 \\ 0 & 0 & 0 & A_{11}-\lambda^2 \end{vmatrix} = 0 \tag{A6}$$

$$\therefore \quad \begin{aligned} \lambda_1 &= -\sqrt{A_{11}} \\ \lambda_2 &= -\sqrt{\frac{1}{2}(A_{22}+A_{33})+\sqrt{\frac{1}{4}(A_{22}-A_{33})^2+A_{23}A_{32}}} \quad , \quad \lambda_5 = -\lambda_1 \\ \lambda_3 &= -\sqrt{\frac{1}{2}(A_{22}+A_{33})-\sqrt{\frac{1}{4}(A_{22}-A_{33})^2+A_{23}A_{32}}} \quad , \quad \lambda_6 = -\lambda_2 \\ \lambda_4 &= -\sqrt{A_{11}} \quad , \quad \lambda_7 = -\lambda_3 \\ & \qquad\qquad\qquad\qquad\qquad\qquad\qquad\quad , \quad \lambda_8 = -\lambda_4 \end{aligned}$$

Here since the solutions with eigenvalues of $\lambda_5, \lambda_6, \lambda_7, \lambda_8$ increase exponentially as y increases, they are invalid. Accordingly there are four independent solutions in the above equation.

On the other hand, the following solution ψ_i is usually assumed to obtain the eigenfunction.

$$\psi_i(y) = \sum_{l=1}^{8} B_{il}\, d_l\, e^{\lambda_l y} \quad , \quad i = 1 \sim 4 \tag{A7}$$

And by inserting (A7) into Equation (A5), the expansion coefficients $\{B_{ij}\}$ are obtained as follows :

$$\{B_{ij}\} = \begin{pmatrix} 1 & B_{12} & B_{13} & 0 & 1 & B_{16} & B_{17} & 0 \\ 0 & 1 & 1 & 0 & 0 & 1 & 1 & 0 \\ 0 & B_{32} & B_{33} & 0 & 0 & B_{36} & B_{37} & 0 \\ 0 & 0 & 0 & 1 & 0 & 0 & 0 & 1 \end{pmatrix} \tag{A8}$$

where

$$B_{1l} = \frac{A_{12}A_{23} + (\lambda_l^{\,2} - A_{22})A_{13}}{(\lambda_l^{\,2} - A_{11})A_{23}} \quad , \quad l = 2,3,6,7$$

$$B_{2l} = 1$$

$$B_{3l} = \frac{\lambda_l^{\,2} - A_{22}}{A_{23}}$$

$$B_{4l} = 0$$

Here d_l is constant numbers determined by the condition of normalization.

Finally, the four independent solutions $\bar{\varphi}_i$ are summarized in the following form.

$$\bar{\varphi}_i^{(l)}(y) = \Lambda_{il}\, e^{\lambda_l y} \quad , \; l = 1 \sim 4 \quad , \quad i = 1 \sim 8 \tag{A9}$$

$$(\Lambda_{ij}) = \begin{pmatrix} 1 & \Lambda_{12} & \Lambda_{13} & 0 & 1 & \Lambda_{16} & \Lambda_{17} & 0 \\ \lambda_1 & \Lambda_{22} & \Lambda_{23} & 0 & -\lambda_1 & \Lambda_{26} & \Lambda_{27} & 0 \\ \Lambda_{31} & \Lambda_{32} & \Lambda_{33} & 0 & -\Lambda_{31} & \Lambda_{36} & \Lambda_{37} & 0 \\ 0 & \Lambda_{42} & \Lambda_{43} & 0 & 0 & \Lambda_{46} & \Lambda_{47} & 0 \\ 0 & \Lambda_{52} & \Lambda_{53} & 0 & 0 & \Lambda_{56} & \Lambda_{57} & 0 \\ 0 & \Lambda_{62} & \Lambda_{63} & 0 & 0 & \Lambda_{66} & \Lambda_{67} & 0 \\ 0 & 0 & 0 & 1 & 0 & 0 & 0 & 1 \\ 0 & 0 & 0 & \Lambda_{84} & 0 & 0 & 0 & -\Lambda_{84} \end{pmatrix}$$

$$\Lambda_{31} = \frac{\bar{a}_{31}}{\lambda_1}$$

$$\Lambda_{84} = \frac{\bar{a}_{87}}{\lambda_4}$$

$* B_{1l} \neq 0 \quad , \quad l = 2,3,6,7$

$$\Lambda_{1l} = 1 \quad , \quad \Lambda_{2l} = \lambda_l \quad , \quad \Lambda_{3l} = \frac{\bar{a}_{31}B_{1l} + \bar{a}_{34}B_{2l} + \bar{a}_{35}B_{3l}}{\lambda_l B_{1l}} \quad ,$$

$$\Lambda_{4l} = \frac{B_{2l}}{B_{1l}} \quad , \quad \Lambda_{5l} = \frac{B_{3l}}{B_{1l}} \quad , \quad \Lambda_{6l} = \lambda_l \Lambda_{5l}$$

$* B_{1l} = 0 \quad , \quad l = 2,3,6,7$

$$\Lambda_{1l} = \Lambda_{2l} = 0 \quad , \quad \Lambda_{3l} = \frac{\bar{a}_{34}B_{2l} + \bar{a}_{35}B_{3l}}{\lambda_l} \quad ,$$

$$\Lambda_{4l} = B_{2l} \quad , \quad \Lambda_{5l} = B_{3l} \quad , \quad \Lambda_{6l} = \lambda_l B_{3l}$$

APPENDIX III. OUTLINE OF THE PRESENT METHOD OF SOLUTION

Usually because of four independent eigenvalues and eigenfunctions , a general solution of the present basic equation is composed with the four independent solutions as follows :

$$\varphi_i(y) = \sum_{l=1}^{4} k_l \, \varphi_i^{(l)}(y) \qquad \text{(A10)}$$

Here each independent solution $\varphi_i^{(l)}(y)$ is obtained by integrating the basic equation from edge to wall . And on the initial values in this integration , we apply the following analytic solution derived in APPENDIX II .

$$\varphi_i^{(l)}(\delta) = \bar{\varphi}_i^{(l)}(\delta) \qquad \text{(A11)}$$

By the way , those independent solutions generally have non-zero values at wall , namely $\varphi_i^{(l)}(0) \neq 0$. Therefore the four expansion coefficients k_l satisfied with the following equation are completely equal to 0 .

$$\varphi_i(0) = \sum_{l=1}^{4} k_l \, \varphi_i^{(l)}(0) = 0 \quad , \quad i = 1,3,5,7 \qquad \text{(A12)}$$

To avoid such trivial situation , we assume the following "pseudo" boundary condition .

At first , let's consider to relax one of the boundary conditions for above four physical quantities . That is , in our method , we tentatively selected the condition for φ_1 . Then we replace it with the following condition for $\varphi_4 = \tilde{p}$. Because we have no boundary condition for φ_4 .

$$\begin{pmatrix} \varphi_3^{(1)}(0) & \varphi_3^{(2)}(0) & \varphi_3^{(3)}(0) & \varphi_3^{(4)}(0) \\ \varphi_4^{(1)}(0) & \varphi_4^{(2)}(0) & \varphi_4^{(3)}(0) & \varphi_4^{(4)}(0) \\ \varphi_5^{(1)}(0) & \varphi_5^{(2)}(0) & \varphi_5^{(3)}(0) & \varphi_5^{(4)}(0) \\ \varphi_7^{(1)}(0) & \varphi_7^{(2)}(0) & \varphi_7^{(3)}(0) & \varphi_7^{(4)}(0) \end{pmatrix} \begin{pmatrix} k_1 \\ k_2 \\ k_3 \\ k_4 \end{pmatrix} \equiv \{\Gamma_{ij}\}\{k_j\} = \begin{pmatrix} 0 \\ 1 \\ 0 \\ 0 \end{pmatrix} \tag{A13}$$

Here we conveniently assumed that the value of φ_4 at wall was equal 1 without lack of generality.

Accordingly the expansion coefficients $k_{j,}$ are obtained as follows :

$$k_l = \sum_{j=1}^{4} \Gamma_{lj}^{-1} \delta_{j2} = \Gamma_{l2}^{-1} \quad , \quad l = 1 \sim 4 \tag{A14}$$

where $\Gamma_{l2}^{-1} \equiv U_{l2} + i V_{l2}$

$$\{U_{ij}\} = \left(\{S_{ij}\}^{-1}\{T_{ij}\} + \{T_{ij}\}^{-1}\{S_{ij}\} \right)^{-1} \{T_{ij}\}^{-1}$$

$$\{V_{ij}\} = -\left(\{S_{ij}\}^{-1}\{T_{ij}\} + \{T_{ij}\}^{-1}\{S_{ij}\} \right)^{-1} \{S_{ij}\}^{-1}$$

$$\{S_{ij}\} \equiv \mathrm{Re}\{\Gamma_{ij}\} \quad , \quad \{T_{ij}\} \equiv \mathrm{Im}\{\Gamma_{ij}\}$$

Next we compose a general solution using these coefficients . At that time , the solution for φ_1 must be satisfied with the following true boundary condition .

$$\varphi_1(0) = \sum_{l=1}^{4} k_l \, \varphi_1^{(l)}(0) = 0 \tag{A15}$$

Therefore to keep this condition , we must improve the values of parameters in the matrix $\{a_{ij}\}$ such as $(\alpha, \beta, \omega, R)$ and estimate the four converged independent solutions through the iterative process and the following Newton Method . After the convergence in this process , we can finally obtain the eignevalues (α, β) and eigenfunctions $\varphi_i(y)$ for stability characteristics .

To simplify our iterative process , first of all , we assumed certain values for $R, \omega, \beta(=\beta_r + i\beta_i)$, and tried to improve the value of $\alpha(=\alpha_r + i\alpha_i)$ only . Generally the solutions at the (n+1)-th state in the iterative process can be expressed as follows :

$$\begin{aligned} \alpha_r^{n+1} &= \alpha_r^{n} + \delta\alpha_r^{n} \\ \alpha_i^{n+1} &= \alpha_i^{n} + \delta\alpha_i^{n} \end{aligned} \tag{A16}$$

where $(\alpha_r^{n}, \alpha_i^{n})$ stands for the solutions at the n-th state and $(\delta\alpha_r^{n}, \delta\alpha_i^{n})$ the modification quantities .

If the (n+1)-th solution satisfies the above true boundary condition , those modification quantities can be estimated under the approximation of neglecting the second order of them as follows :

$$\begin{pmatrix} \delta\alpha_r{}^n \\ \delta\alpha_i{}^n \end{pmatrix} = -\begin{pmatrix} p_{11} & p_{12} \\ p_{21} & p_{22} \end{pmatrix}^{-1} \begin{pmatrix} \mathrm{Re}\left(\varphi_1{}^n(0)\right) \\ \mathrm{Im}\left(\varphi_1{}^n(0)\right) \end{pmatrix}$$

where

$$p_{11} \equiv \left[\frac{\partial\,\mathrm{Re}\left(\varphi_1{}^n(0)\right)}{\partial\,\alpha_r}\right]_{(\alpha_r{}^n,\alpha_i{}^n)} = p_{22} \quad , \quad p_{21} \equiv \left[\frac{\partial\,\mathrm{Im}\left(\varphi_1{}^n(0)\right)}{\partial\,\alpha_r}\right]_{(\alpha_r{}^n,\alpha_i{}^n)} = -p_{12}$$

In calculating the derivatives p_{ij}, we used the numerical approach based on the approximation of the modification $\Delta\alpha_r = \varepsilon\alpha_r$ *and* $\varepsilon \approx 10^{-3} \sim 10^{-5}$.

APPENDIX IV. ORTHONORMALIZATION TECHNIQUE BY GRAM-SCHMIDT

Since numerical integration generally produces an error, the orthogonarity of our independent solutions in our method is reduced. To remove this reduction, that is, to keep the orthogonality of the solutions, it is well-known that the following replacement at each integration step for y is effective[3].

$$X^{(l)} \equiv \left\{\varphi_i{}^{(l)}\right\} \Rightarrow Y^{(l)} \quad , \quad l = 1 \sim 4 \quad , \quad i = 1 \sim 8$$

$$Y^{(1)} = \frac{X^{(1)}}{\left|X^{(1)}\right|}$$

$$Y^{(2)} = \frac{\left(X^{(2)} - C_{12}Y^{(1)}\right)}{\left|X^{(2)} - C_{12}Y^{(1)}\right|}$$

$$Y^{(3)} = \frac{\left(X^{(3)} - C_{13}Y^{(1)} - C_{23}Y^{(2)}\right)}{\left|X^{(3)} - C_{13}Y^{(1)} - C_{23}Y^{(2)}\right|}$$

$$Y^{(4)} = \frac{\left(X^{(4)} - C_{14}Y^{(1)} - C_{24}Y^{(2)} - C_{34}Y^{(3)}\right)}{\left|X^{(4)} - C_{14}Y^{(1)} - C_{24}Y^{(2)} - C_{34}Y^{(3)}\right|}$$

$$C_{ij} \equiv Y^{(i)*}X^{(j)}$$

where $*$ denotes complex conjugate.

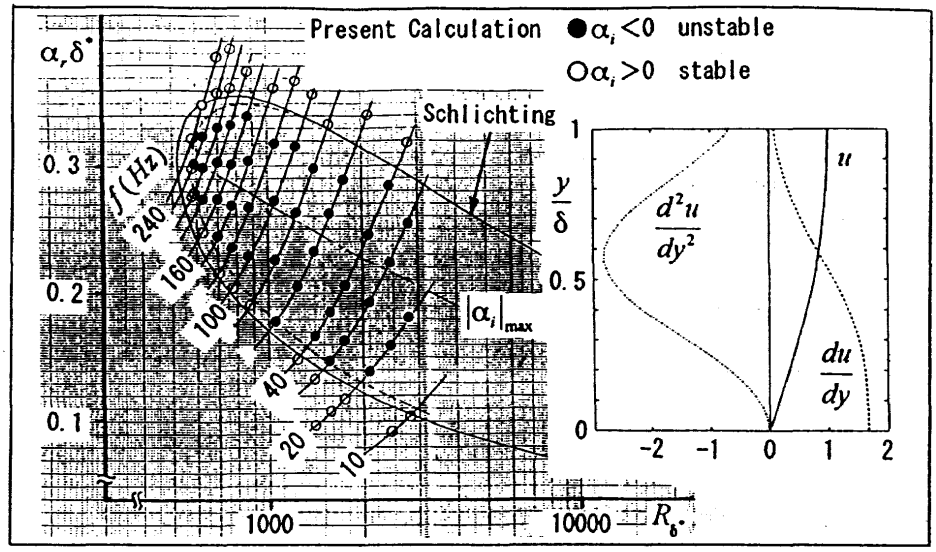

Fig. 1 Stability characteristics of flat plate boundary layer : M = 0

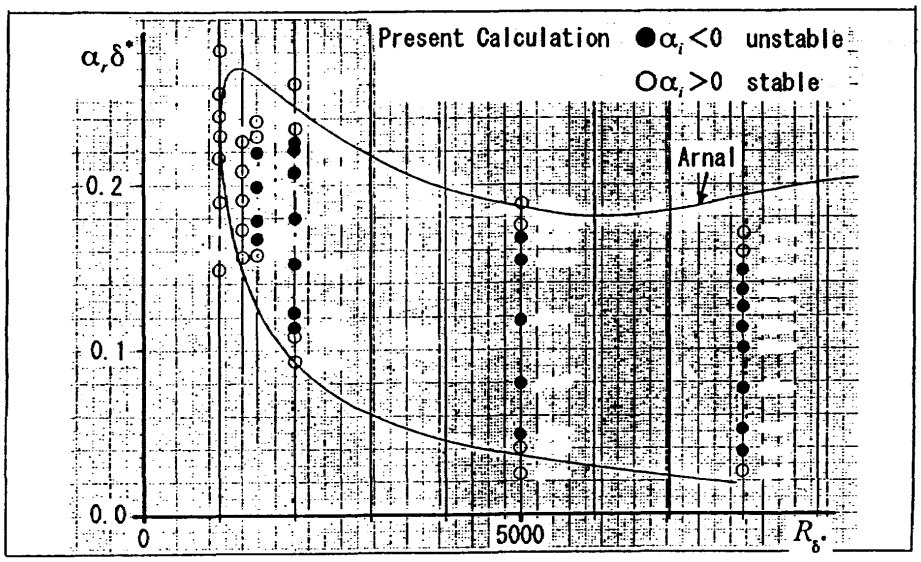

Fig. 2 Stability characteristics of flat plate boundary layer : M = 2.2

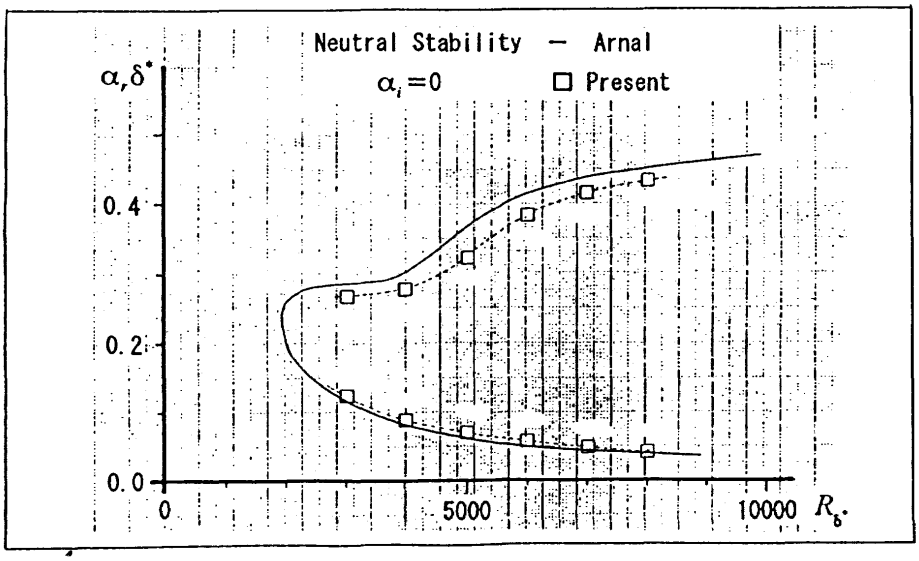

Fig. 3 Stability characteristics of flat plate boundary layer : M = 3.0

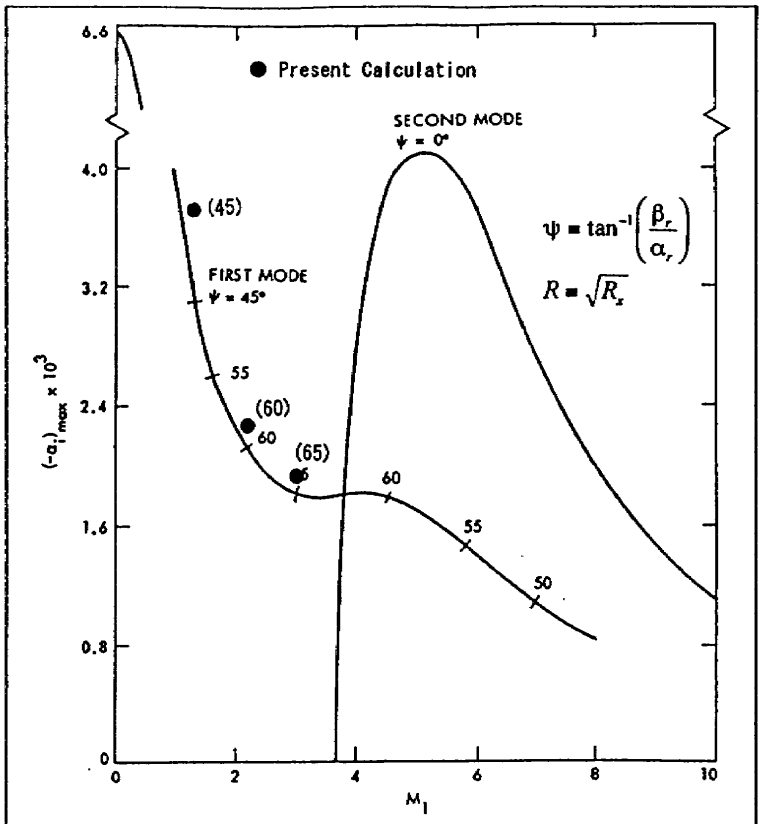

Effect of Mach number on maximum spatial amplification rate at $R = 1500$. Insulated wall.

(Ref : Mack,L.M., AIAA J. Vol.13, No.3, 1975, pp.278-289)

Fig.4 Maximum amplification rate of compressible flat plate boundary layer

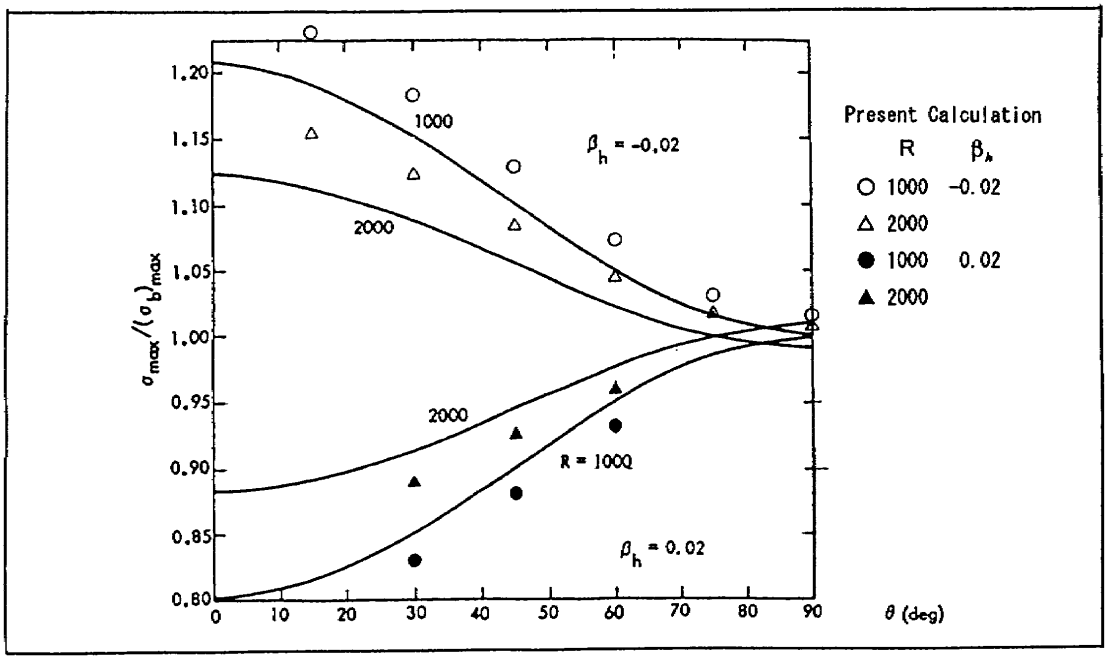

(Ref : Mack,L.M., AGARD Special Course on Stability and Transition , 1984)

Fig.5 Maximum amplification rate of Falkner-Skan-Cooke boundary layer

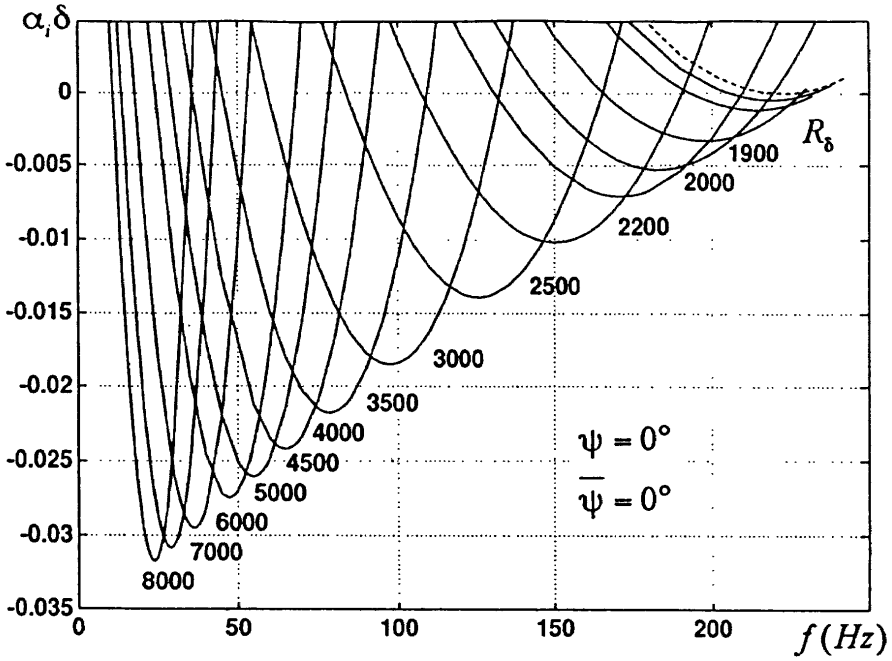

Fig. 6 Estimated amplification rate of Blasius boundary layer

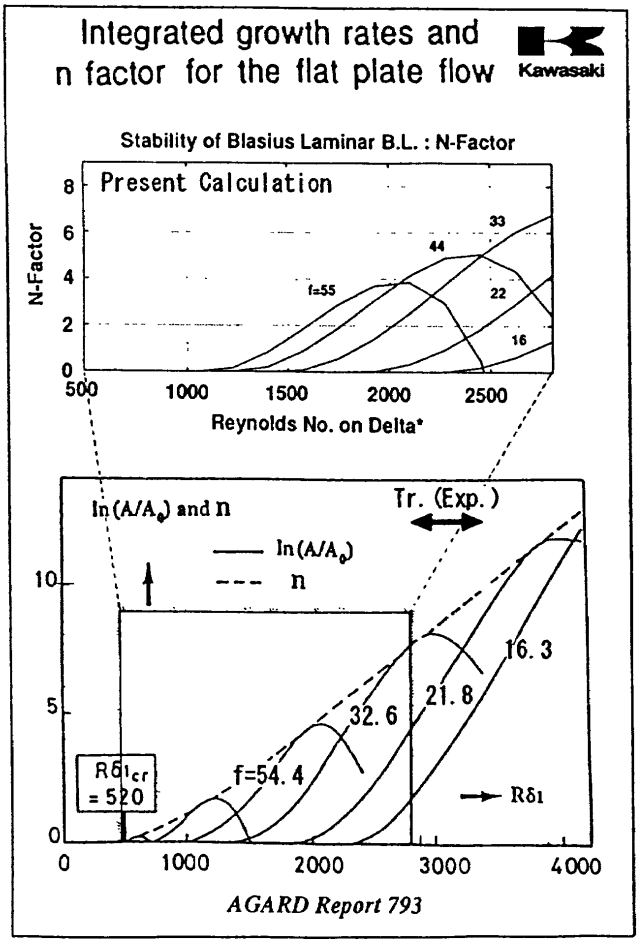

Fig. 7 Estimated N-factor of Blasius boundary layer

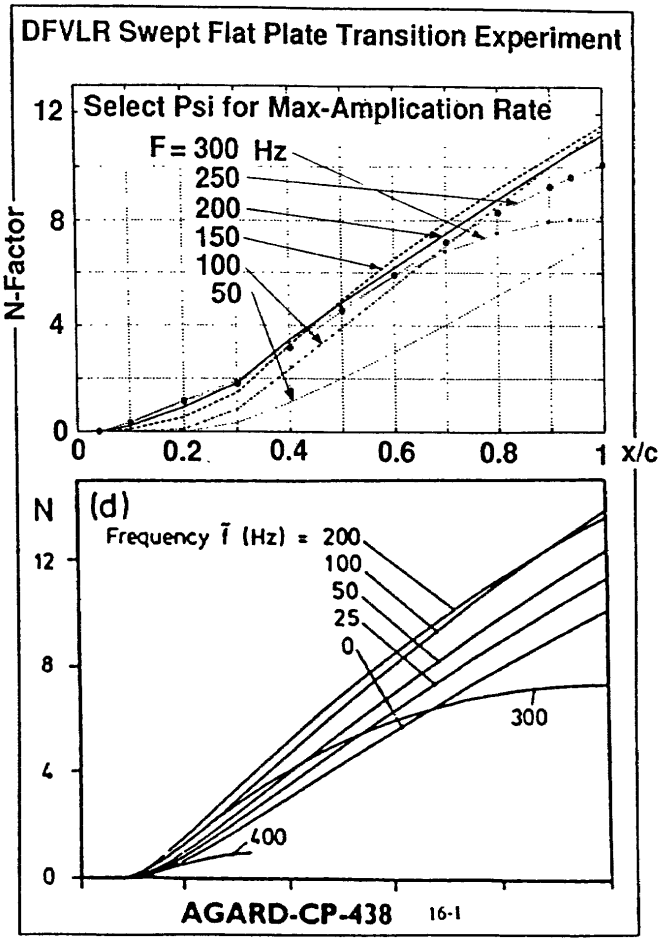

Fig. 8 Estimated N-factor of Falkner-Skan-Cooke boundary layer

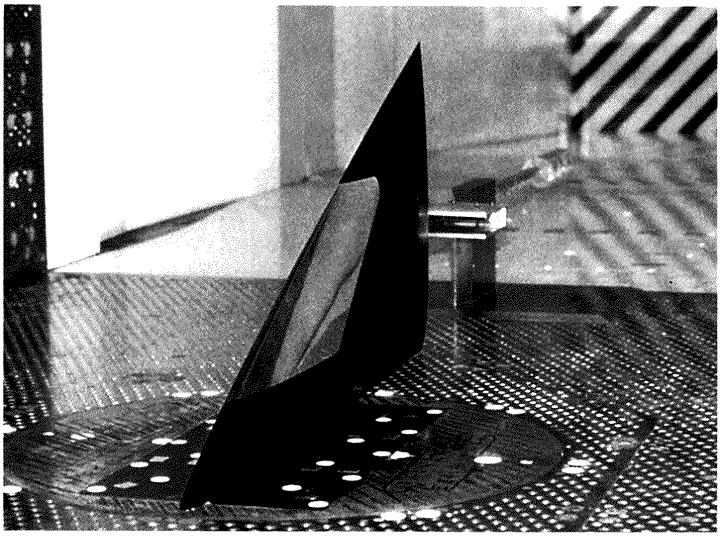

Max. Chord : ℓ=1072.25 mm
Semi-span : s=500 mm
L.E. Sweep : Λ_{LE}=65°
Thick. Ratio : t/c=0.05
Suction Area : $0.03 \leqq x/c \leqq 0.3$
$0.2 \leqq y/s \leqq 0.6$
dia. d=0.1mm
About 60,000 holes

Fig. 9 Wind tunnel model for supersonic laminar flow control test

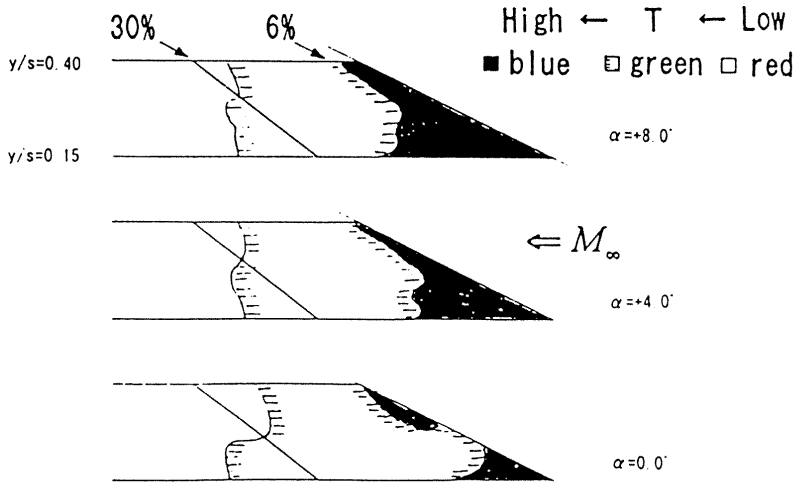

Fig. 10 Sketch on visualization of surface temperature

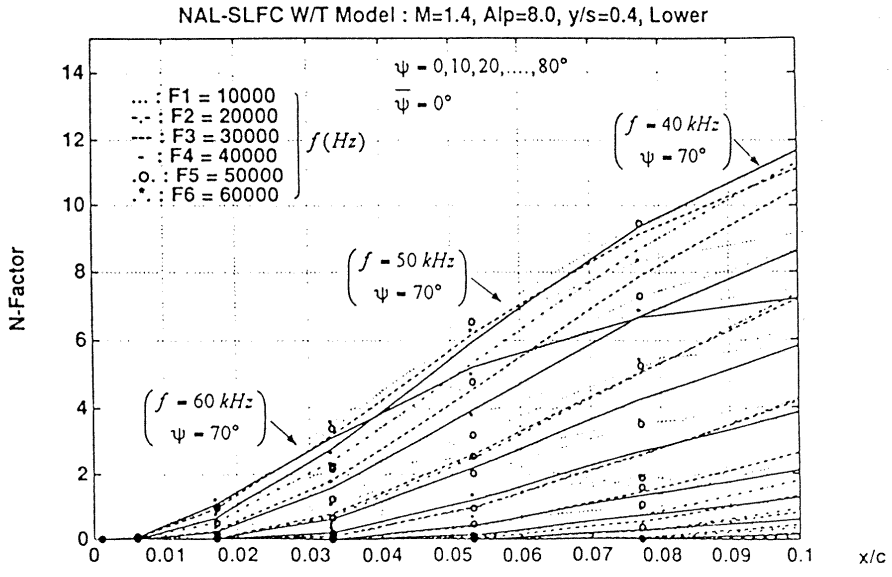

Fig. 11 Estimated N-factor on NAL-SLFC wind tunnel test